HIGH-EFFICIENCY AMORPHOUS SILICON AND NANOCRYSTALLINE SILICON BASED SOLAR CELLS AND MODULES

Quarterly Technical Progress Report
August 1 through October 31, 2007

S. Guha and J. Yang
United Solar Ovonic LLC
Troy, Michigan

NREL Technical Monitor: Bolko von Roedern

Prepared under Subcontract No. ZXL-6-44205-14

Preface

This Quarterly Report covers the work performed by United Solar Ovonic LLC under the Thin Film Partnership Subcontract No. ZXL-6-44205-14 for the period from August 1 to October 31, 2007. The following personnel participated in this research program.

A. Banerjee, E. Chen, G. DeMaggio, S. Guha (Principal Investigator), B. Hang, M. Hopson, N. Jackett, J. M. Owens, J. Noch, T. Palmer, G. Pietka, B. Sivec, L. M. Sivec, D. Wolf, B. Yan, J. Yang (Co-Principal Investigator), G. Yue, K. Younan, and X. Xu.

Collaboration with the National Renewable Energy Laboratory is greatly acknowledged.

Executive Summary

Because of realignment of the Thin Film Partnership Program (TFPP) with the Solar America Initiative Program (SAI), some of the tasks in the original TFPP program were instructed not to continue. Based on the modified statement of work, we have carried out the following activities.

1. We conducted collaboration work with the analytical group and thin film silicon group of the National Renewable Energy Laboratory and carried out a systematic study of microstructures of mixed-phase hydrogenated silicon solar cells. We have previously reported the nanocrystalline cone formation in the mixed-phase materials. In this quarter, we continued to characterize mixed-phase films made with various hydrogen dilutions using Raman spectroscopy, AFM, conductive-AFM, and X-TEM. However, the investigation has not been completed. We shall report the results in the next quarterly report.

2. We optimized a-Si:H top cells in the regime very close to the amorphous/nanocrystalline transition. In order to keep the material still in the amorphous phase through the entire intrinsic layer thickness, hydrogen dilution profiling was used. A high V_{oc} of 1.055 V has been achieved in this study.

3. We continued to optimize a-SiGe:H single-junction solar cells; the a-SiGe:H with high Ge contents is important yet challenging for device optimization. In this quarter, we focused on the optimization of a-SiGe:H single-junction cells with a V_{oc} between 0.65 V and 0.70V, which is normally used as the bottom cell in an a-Si:H/a-SiGe:H/a-SiGe:H triple-junction solar cell.

4. In order to achieve high efficiency multi-junction solar cells, we need to improve back reflectors to enhance the light trapping effect. In this quarter, we continue to optimize Ag/ZnO back reflectors and compared the a-SiGe:H solar cells made on various back reflectors. It appears that when a thin ZnO layer is used, textured Ag is needed. On the other hand, when the ZnO layer is thick enough to provide sufficient light scattering, a specular Ag layer results in an optical enhancement better than a textured Ag layer. We also carried out a study for estimating the optical enhancement in a-SiGe:H solar cells. We proposed a calculation method for the optical enhancement and found that the optimized Ag/ZnO back reflector results in an optical enhancement 20 to 30 times greater in the long wavelength region.

1. Hydrogenated Amorphous Silicon Solar Cells Made Close to the Amorphous to Nanocrystalline Transition

1. 1. Introduction

Hydrogen dilution is used as a key technique for achieving the transition from amorphous to nanocrystalline phase. Although the mechanism of hydrogen dilution induced phase transition is not clear [1], both amorphous and nanocrystalline silicon materials and solar cells made close to the transition region showed superior properties and performance [2, 3]. On the amorphous side, the improvement in solar cell performance is believed to benefit from the inclusion of nano-grains or medium-range-ordered structures [4]. a-Si:H solar cells made with very high hydrogen dilution showed higher open circuit current voltages (V_{oc}) and fill factors than those made with non-diluted or lower hydrogen dilutions. However, if the hydrogen dilution exceeds a certain value, the V_{oc} drops dramatically, transitioning from the amorphous to nanocrystalline phase [5]. Another phenomenon was the evolution of the nanocrystalline structure. It was found that the nanocrystallinity increases with the film thickness [6-8], causing problems in the nc-Si:H cell performance. A hydrogen dilution profiling scheme, which dynamically reduces the hydrogen dilution during film growth, has been developed to control the nanocrystalline evolution, and is confirmed to be an effective method for improving the nc-Si:H cell efficiency [9]. For a-Si:H, the nanocrystalline evolution could also cause problems in solar cell performance. Under a constant hydrogen dilution condition, the initial growth could be far from the amorphous to nanocrystalline transition region. When the film thickness continues to grow, entering the amorphous to nanocrystalline transition region, the resulting solar cells exhibit a large reduction in V_{oc} [5]. Therefore, using hydrogen dilution profiling during the a-Si:H deposition could also be an effective way to improve the cell performance. Based on this hypothesis, we have carried out a systematic study of thin a-Si:H cells, which are normally used as the top cells in a-Si:H/a-SiGe:H/a-SiGe:H triple-junction structures.

Formatted: Bullets and Numbering

Experimental details

a-Si:H *n-i-p* solar cells were made using RF glow discharge at a low rate of ~1 Å/s on bare stainless steel (SS) substrates. Indium-Tin-Oxide (ITO) dots with an active-area of 0.05 and 0.25 cm^2 were deposited on the *p*-layer as the top transparent contact. The deposition parameters were systematically optimized, especially the hydrogen dilution ratio, hydrogen dilution profiling, and substrate temperature. The solar cell performance was characterized using current density versus voltage (J-V) measurements under an AM1.5 solar simulator at 25 °C, and quantum efficiency (QE) measurements under the short-circuit condition. In order to illustrate the amorphous to nanocrystalline transition at different areas on one substrate, the J-V data presented here are raw measurements under the AM1.5 solar simulator without referring to the short circuit current density from the QE data. Therefore, attention should be paid to the open circuit voltage (V_{oc}) and fill factor (FF), not the J_{sc}.

1. 3. Results and discussion

We first increased the hydrogen dilution to reach the amorphous to nanocrystalline transition regime. As previously reported, the geometry of the cathode design causes a non-uniform distribution of crystallinity over the substrate area [10, 11]. It was observed that in the amorphous to nanocrystalline transition regime, the nanocrystalline formation appears at the corners or edge first, while the center area exhibits more amorphous component. We used this phenomenon to monitor the phase transition. Table I lists two sets of a-Si:H top cells made in the transition region. The first three samples were made with a constant hydrogen dilution ratio. Sample 16341 is a baseline cell, which showed a V_{oc} of 1.036 V in the center, indicating good a-Si:H properties. However, at the edge, the V_{oc} drops to 0.786 V, resulting from the mixed-phase formation. Sample 16345 was made under the same condition as Sample 16341 except for a thinner intrinsic layer. As typically observed, for a reduced intrinsic layer thickness, the V_{oc} increases to 1.043 V at the center and 0.995 at the edge, confirming the nanocrystalline evolution with the thickness, especially at the edge. At the same time, the FF is also improved. Sample 16346 was made under the same condition as Sample 16345 except the substrate temperature (T_s) was reduced by 25 °C. As expected, the lower substrate temperature results in an even higher V_{oc} but smaller J_{sc}.

Table I. J-V characteristics of a-Si:H top cells made with flat hydrogen dilution and profiled hydrogen dilution.

Sample No	Position	Eff (%)	J_{sc} (mA/cm^2)	V_{oc} (V)	FF	Comments
16341	Center	6.75	9.34	1.036	0.697	Constant H dilution Baseline
	Middle	6.57	9.55	1.030	0.667	
	Edge	4.12	9.04	0.786	0.580	
16345	Center	6.28	7.97	1.043	0.757	Constant H dilution with thin i-layer
	Middle	6.19	7.98	1.042	0.745	
	Edge	5.61	8.14	0.995	0.693	
16346	Center	5.94	7.77	1.049	0.729	Constant H dilution with thin i-layer and low T_s
	Middle	5.94	7.79	1.047	0.729	
	Edge	5.40	7.46	1.036	0.698	
16140	Center	7.30	9.92	1.034	0.712	Profiled H dilution Baseline
	Middle	7.12	9.92	1.031	0.692	
	Edge	5.48	9.68	0.880	0.644	
16343	Center	6.25	8.34	1.027	0.730	Profiled H dilution with thin i-layer
	Middle	6.31	8.48	1.030	0.723	
	Edge	5.53	8.36	0.964	0.686	
16344	Center	6.26	7.92	**1.055**	0.748	Profiled H dilution with thin i-layer and low T_s
	Middle	5.90	7.60	1.048	0.740	
	Edge	4.2	7.32	0.916	0.626	

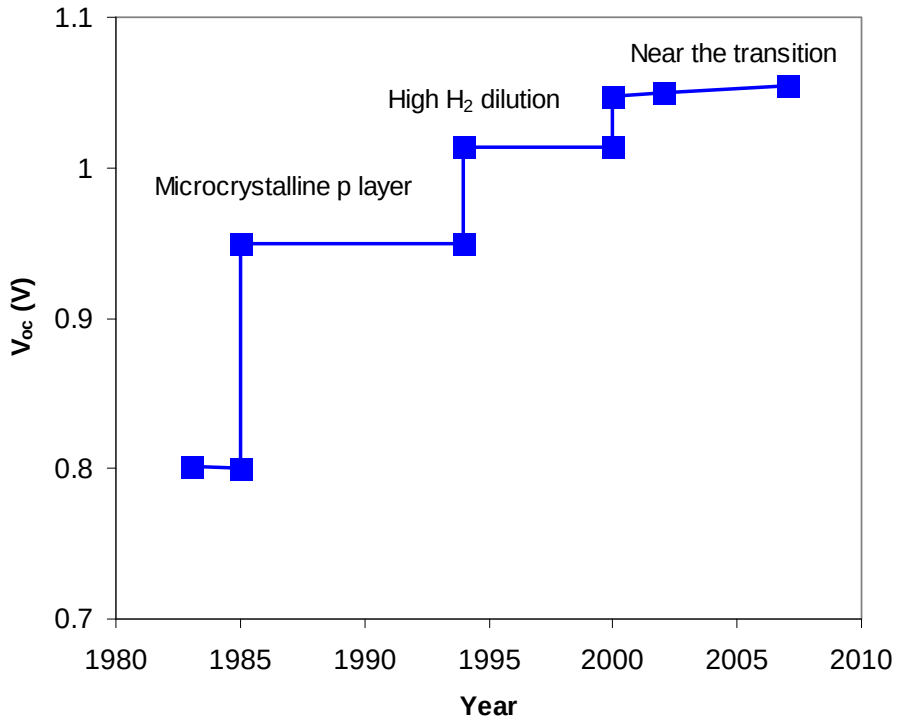

Figure 1. United Solar's historical improvements in open-circuit voltage in a-Si:H solar cells when different technologies were invented and used.

The lower three samples in Table I were made with a hydrogen dilution profiling with a dynamically reduced hydrogen dilution, where the hydrogen flow rate was linearly decreased with time. The average hydrogen dilution of this set was about 10% lower than the first set. When the same average dilution ratio was used, the cells made with hydrogen dilution profiling became mixed-phased solar cells, indicating the very high hydrogen dilution at the initial stage of deposition could produce a nc-Si:H seed layer for subsequent deposition. Therefore, the average hydrogen dilution has to be reduced when a hydrogen dilution profiling is used for a-Si:H deposition. Sample 16140 was a baseline cell made with hydrogen dilution profiling, which performs better than Sample 16341 made with constant hydrogen dilution. Reducing the thickness of the intrinsic layer by simply reducing the deposition time with the same ratio of hydrogen profiling did not increase the V_{oc} as observed in the samples with the constant hydrogen dilution ratio. An explanation could be that the initial hydrogen dilution was too high in the profiled sample and the initial growth has more effect for the thinner samples than for the thicker samples. By reducing the substrate temperature, the V_{oc} is improved dramatically, and we achieved an initial V_{oc} of 1.055 V, which is the highest value achieved in our laboratory. Currently, we are working on fine tuning the hydrogen dilution profiling to obtain an even higher V_{oc}. Figure 1 shows the historical evolution of V_{oc} when different processing techniques were used. Normally, it is believed that the V_{oc} is limited by the properties of the intrinsic layer and the quality of interfaces, especially the *i/p* interface.

The upper limit of V_{oc} is the built-in potential, which is around 1.1-1.2 V. Although we may still have room for further improvement, the new record has approached the built-in potential.

1. 4. Summary

In this quarter, we continued to optimize a-Si:H top cells using the hydrogen dilution technique and tried to approach the amorphous to nanocrystalline transition region. The hypothesis of this method is based on the observations that i) a-Si:H cells made under high hydrogen dilution perform better than those made with low hydrogen dilution and ii) the nanocrystallinity increases with film thickness when the nanocrystalline formation appears. By reducing the hydrogen dilution during the intrinsic layer deposition, we may keep the material structure close to the transition region but in the amorphous phase throughout the thickness of the intrinsic layer. The experimental data showed that the samples made with the hydrogen dilution profiling displayed a noticeable improvement over the constant hydrogen dilution. In this study, we have achieved an initial V_{oc} of 1.055 V for an a-Si:H solar cell. Currently, we are working on further optimization of the hydrogen dilution profiling.

2. Optimization of a-SiGe:H Alloy Component Cells and Optimization of Ag/ZnO Back Reflector for Light Trapping in a-SiGe:H Cells

2. 1. Introduction

The current product from United Solar is based on the spectrum splitting a-Si:H/a-SiGe:H/a-SiGe:H triple-junction cell structure on back reflector coated stainless steel substrates. As shown previously, the major challenge for improving the efficiency further lies on the quality of the a-SiGe:H bottom cell, where the Ge content is higher than the a-SiGe:H middle cell [12]. The decline of a-SiGe:H quality with the increase of Ge content is mainly caused by the inefficient Ge dangling bond passivation. In this quarter, we focused on the optimization of a-SiGe:H bottom cells on bare stainless steel (SS) and on Ag/ZnO back reflector coated SS substrates.

One important method to increase the thin film solar cell efficiency is using textured back reflector (BR) to enhance the optical absorption. When light reaches the substrates in a thin film solar cell, the light is either reflected back to the cell or absorbed by the substrate. In order to reduce the absorption in the substrate and enhance the reflection, metal layers such as Al and Ag are used as a back reflector, and the metal surface is textured for enhanced light scattering. In addition, a dielectric layer such as ZnO is used for additional texturing and more efficient light scattering. Furthermore, it has been reported that a flat metal layer and a textured ZnO layer are the best combination because the flat metal surface can reduce the plasmon absorption at the metal/dielectric interface [13]. In this quarter, we have systematically studied the light trapping effect of Ag/ZnO back reflectors with flat or textured Ag, as well as different ZnO thickness.

Although a significant amount of work has been done on the optimization of the light trapping effect [14, 15], a reliable calculation method of the optical enhancement, defined as the numbers of paths that light can travel in the solar cells, for a-SiGe:H solar cells, has not been established. An early work by Yablonovitch showed that the maximum optical enhancement is $4n^2$ [16], where n is the optical index of the thin film semiconductor layer. The $4n^2$ factor is called Yablonovitch enhancement for stochastic light trapping. In silicon, this number is about 50.

In this quarter, we compared the QE and reflection curves of a-SiGe:H bottom cells made on SS and Ag/ZnO back reflector substrates and proposed an estimation method for calculating the optical enhancement.

2. 2. Optimization of a-SiGe:H bottom cells

In this quarter, we first optimized a-SiGe:H bottom cells on SS substrates. Table II lists the J-V characteristics of a-SiGe:H bottom cells on SS substrates. Normally we characterize a-SiGe:H bottom cells using both the AM1.5 and red lights. For a-SiGe:H bottom cells on SS, a 530-nm long pass filter is used. A benchmark of P_{max} under the red

Table II. Typical J-V characteristics of a-SiGe:H bottom cells on stainless steel substrates, where the data were measured under AM1.5 illumination and with a 530-nm long-pass filter. The J_{sc} data were calculated from convoluting the QE curves with the AM1.5 spectrum. The FF under the blue and red lights was measured under narrow band pass filters.

Sample	Light source	P_{max} (mW/cm^2)	J_{sc} (mA/cm^2)	V_{oc} (V)	FF		
					AM1.5	Blue	Red
16332	>530 nm	4.42	10.81	0.662	0.618		
	AM1.5	7.08	16.71	0.679	0.624	0.694	0.635
16337	>530 nm	4.46	11.11	0.662	0.607		
	AM1.5	6.98	16.88	0.677	0.611	0.699	0.640
16388	>530 nm	4.45	11.06	0.665	0.601		
	AM1.5	6.88	16.75	0.680	0.604	0.682	0.624
16339	>530 nm	4.40	10.48	0.660	0.636		
	AM1.5	6.53	16.12	0.675	0.600	0.701	0.665
16366	>530 nm	4.52	10.90	0.666	0.622		
	AM1.5	7.23	16.90	0.682	0.627	0.692	0.640

light illumination is 4 mW/cm^2. Although the cell performance has not reached the best results achieved previously [12], the cells showed very good performances. We also listed the FF measured under weak blue and red lights from a white light source through narrow band pass filters. The blue light provides information for the region near the *i/p* interface, while the red light measures the quality of the intrinsic layer. It appears that the red FF is much lower than the blue FF, indicating that the material quality in the intrinsic layer needs to be improved further. In addition, a proper Ge profiling may also improve the cell performance further.

We used the recipe of a-SiGe:H bottom cells on SS to start optimizing cells on Ag/ZnO back reflectors. Table III lists the J-V characteristics of a-SiGe:H bottom cells made with the same recipe as Sample 16332. The first two samples in Table III serve as baseline samples. The Ag/ZnO back reflector from a roll-to-roll machine was used for Sample 16387. Then, we compared the cell performance for the cells on Ag/ZnO back reflectors with flat and textured Ag layers. First, a pair of cells (16382 and 16380) on the Ag/ZnO back reflectors with a thinner ZnO showed that the textured Ag layer produces much higher J_{sc} than the flat Ag layer, especially for the long wavelength region. However, when a thick ZnO layer was used, the Ag/ZnO with the flat Ag layer produced a similar or slightly higher J_{sc} than the textured Ag layer.

In order to investigate the optical loss mechanisms of a-SiGe:H bottom cells on various Ag/ZnO back reflectors, we measured the total reflection of the substrates using an integrating sphere. Figure 2 (a) shows the total reflection spectra of various substrates. First, the SS has a relatively flat reflection spectrum with a reflectivity ranging from 0.5-0.6, which slightly increases with the increase of wavelength. The Ag/ZnO back reflectors show a large reflection minimum in the short wavelength region around 350-

400 nm, which has been identified as the plasmon absorption at the Ag/ZnO interface. It appears that the flat Ag results in a higher reflection than the textured Ag layer, presumably caused by the reduced plasmon absorption. The enhanced reflection by the flat Ag is observed in both cases with thinner and thicker ZnO layers. In addition to the loss by plasmon absorption, the absorption in the ZnO layer also plays a significant role, especially in the long wavelength region. The lower reflectivity of the Ag/ZnO back reflectors with thicker ZnO could be mainly caused by the extra absorption of ZnO. Figure 2 (b) plots the average reflections in the short (300-650 nm), long (650-1000 nm) and entire (300-1000 nm) wavelength regions. On the average, the thinner ZnO layer results in higher reflection in the whole wavelength region.

The light trapping effect not only depends on the total reflection from the back reflector, but also on the scattering at the semiconductor/dielectric interface as well as the dielectric/metal interface. From Table III, one can see that the cells on the Ag/ZnO back reflectors with a thinner ZnO layer showed lower J_{sc}, especially for the one with a flat Ag layer. It is clear that for the Ag/ZnO back reflector with a thin ZnO layer, the texture of the Ag layer is very important because it provides the effect of scattering. Figure 3 (a) compares the quantum efficiency and reflection curves of the two cells on Ag/ZnO back

Table III. J-V data of a-SiGe:H bottom cells made with the same recipe as in Sample 16332 but on flat stainless steel and different Ag/ZnO back reflectors. The long wavelength performance was measured with a 530-nm long pass filter for the cells on stainless steel substrates and with a 630-nm long pass filter for the cells on Ag/ZnO back reflectors.

Run #	Light	J_{sc} (mA/cm^2)	V_{oc} (V)	FF	P_{max} (mW/cm^2)	Substrate	Comment
16332	AM1.5	16.71	0.679	0.624	7.08	SS	Flat
	>530 nm	10.81	0.662	0.618	4.42		
16366	AM1.5	16.91	0.682	0.627	7.23	SS	Flat
	>530 nm	10.90	0.666	0.627	4.52		
16387	AM1.5	22.81	0.680	0.599	9.29	Ag/ZnO	Textured Ag
	>630 nm	10.58	0.646	0.601	4.11	5MW2040	0.6 μm ZnO
16382	AM1.5	21.01	0.662	0.585	8.14	Ag/ZnO	Flat Ag
	>630 nm	9.01	0.624	0.585	3.29	R8568	0.5 μm ZnO
16380	AM1.5	22.61	0.672	0.562	8.54	Ag/ZnO	Textured Ag
	>630 nm	10.35	0.638	0.569	3.76	R8567	0.5 μm ZnO
16402	AM1.5	23.78	0.689	0.610	9.99	Ag/ZnO	Flat Ag
	>630 nm	11.24	0.661	0.619	4.60	R8578	2.0 μm ZnO
16413	AM1.5	23.53	0.686	0.617	9.96	Ag/ZnO	Flat Ag
	>630 nm	10.94	0.655	0.613	4.39	R8578	2.0 μm ZnO
16357	AM1.5	23.33	0.699	0.619	10.09	Ag/ZnO	Textured Ag
	>630 nm	10.89	0.667	0.619	4.50	R8483	2.0 μm ZnO
16364	AM1.5	23.55	0.696	0.597`	9.79	Ag/ZnO	Textured Ag
	>630 nm	11.01	0.665	0.602	4.41	R8562	2.0 μm ZnO

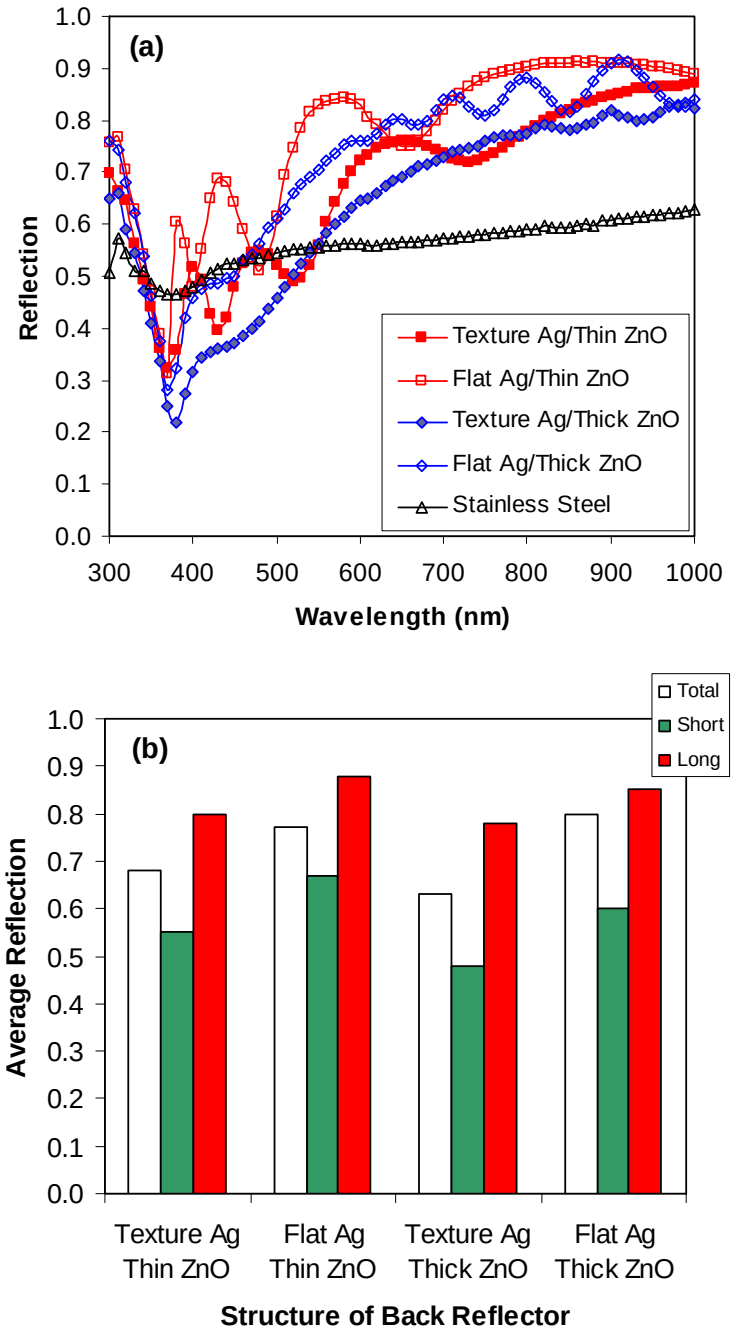

Figure 2. (a) Total reflection spectra of stainless steel and various Ag/ZnO back reflectors; (b) the average reflection for various spectrum regions.

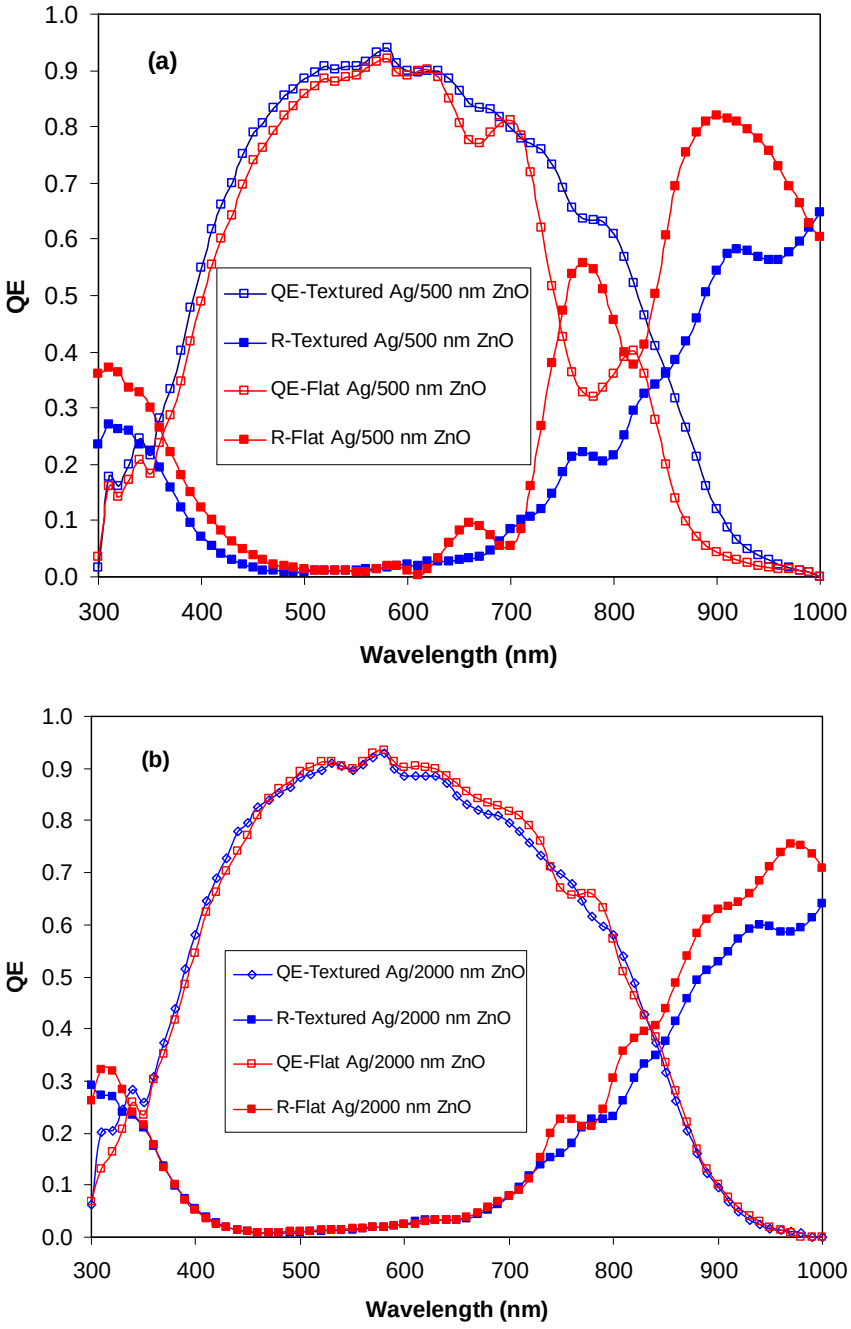

Figure 3. (a) A comparison of QE and R curves of a-SiGe:H solar cells on Ag/ZnO with textured Ag and flat Ag layers and with a 500-nm thick ZnO; (b) the same comparison except the ZnO layer is 2000-nm thick.

reflectors with the thinner ZnO layer. The long wavelength reflection is much higher from the cell with a flat Ag layer than from the one with a textured Ag layer. Correspondingly, the long wavelength quantum efficiency is lower in the cell with a flat Ag layer than that with a textured ZnO layer.

The comparison of the cells on Ag/ZnO with thicker ZnO layers reveals a different picture. From Table III, one can see that the flat Ag layer produces a J_{sc} similar to (or slightly higher than) the cells on Ag/ZnO back reflector with the textured Ag layer; even though the scattering from the back reflector with the textured Ag layer is high as indicated by the suppressed interference fringes in Figure 2 (a). Fig. 3 (b) shows the comparisons of the quantum efficiency and reflection curves of a-SiGe:H cells on Ag/ZnO back reflectors with either flat Ag or textured Ag layer, where the ZnO thickness is 2.0 μm. The QE curves are very similar except for clear interference fringes in the sample with flat Ag, indicating lower scattering with the flat Ag layer. The reflection curves still show that the cell with the flat Ag layer has high reflection in the long wavelength region. For the samples with the thick ZnO, the flat Ag has a lower absorption loss in the metal/dielectric interface, but the scattering is also lower. On the other hand, the textured Ag layer provides higher scattering, but the absorption is higher than the samples with a flat Ag layer.

To summarize the quantum efficiency and reflection results, we can make the following observations. First, for Ag/ZnO back reflectors with a thinner ZnO, the textured Ag is definitely a necessary component for providing sufficient light scattering. Second, for the Ag/ZnO back reflectors with a thicker ZnO layer, the quantum efficiency is similar for the samples with flat Ag and textured Ag layers. The flat Ag layer reduces the plasmon absorption in the metal/dielectric interface, but does not provide high light scattering as obtained from the textured Ag layer. Third, a thicker ZnO also improves the V_{oc} slightly, which could be due to the reduction of the density of sharp features on the ZnO surface as measured by AFM microscopic images [15]. Overall, the long wavelength (>630 nm) P_{max} has been improved from 3.8 mW/cm^2 to 4.6 mW/cm^2 when the Ag/ZnO is changed from flat Ag and thin ZnO to flat Ag and thick ZnO layers. The trend is clear that a flat Ag layer with a thicker ZnO having sufficient texture is the most desirable structure for high efficiency solar cells.

2. 3. Calculation of optical enhancement in a-SiGe:H cells on Ag/ZnO back reflector

2.3.1. Methodology

In order to obtain the optical enhancement factor, we have to establish a baseline for reference. Thin film solar cells on flat stainless steel substrates should be good baselines. Therefore, the optical enhancement obtained in this way is the effective increase of the absorption length for reaching the quantum efficiency ratio of solar cells deposited on back reflectors over stainless steel substrates at different wavelengths. The procedure includes a comparison of the quantum efficiency curves of a-SiGe:H single-junction solar cells made with the same recipe on bare stainless steel substrate and

Ag/ZnO back reflectors. A mathematical calculation procedure is proposed with certain assumptions.

2.3.2. Mathematical Formulation

First, we calculate the quantum efficiency as a function of absorption coefficient and cell thickness. Assume $N_0(\lambda)$ of photons with wavelength λ get into the solar cell. The absorption coefficient for this wavelength is α. When we assume the generation rate is 100%, the density of electron/hole pairs generated at the position of x is,

$$N(x,\lambda) = N_0(\lambda)\exp(-\alpha x). \quad (1)$$

The amount electron/hole pairs (photons absorbed) generated between x and $x+dx$ is,

$$dN(x,\lambda) = \alpha N_0 \exp(-\alpha x)dx. \quad (2)$$

For the cells on stainless steel substrates, we assume that the light reaches the substrates and reflects back with a reflection coefficient R. We also assume that the reflected light will come out of the cell when it reaches the top surface, which means there are only two paths (one can consider more paths with a high order polynomial approach). In this case, we integrate eq.(2) over the intrinsic layer thickness L for the direct incident beam and the reflection beam and obtain,

$$N(\lambda) = N_0\int_0^L \alpha\exp(-\alpha x)dx + RN_0\exp(-\alpha L)\int_L^0 \alpha\exp(-\alpha(L-x))dx. \quad (3)$$

$$N(\lambda) = N_0\left[(1-\exp(-\alpha L))(1+R(\exp(-\alpha L)))\right]. \quad (4)$$

We assume that there is no recombination loss, which means every photon-generated electron/hole pair is collected and contributes to the quantum efficiency (Q_{SS}) measurements. In this case, the Q_{SS} is the ratio of absorbed photons to total incident photons. Then, we obtain,

$$R\left[\exp(-\alpha L)\right]^2 + (1-R)\exp(-\alpha L) + (Q_{SS}-1) = 0, \quad (5)$$

From the positive solution of this quadratic equation, we obtain,

$$\alpha L = -\ln\left\{\frac{\sqrt{(1-R)^2 + 4R(1-Q_{SS})} + (R-1)}{2R}\right\}. \quad (6)$$

In the case of solar cells on a textured back reflector, we assume the reflection coefficient at the surface of BR is one hundred percent, and the reflection at the top surface is also one hundred percent (total reflection). Although these assumptions are not realistic, the losses at the interface (by absorption in the interface or escaping out at the top surface) are considered as the reduction of the effective paths of the trapped light. Therefore, the estimated optical enhancement is the lowest limitation. With these assumptions, we define an effective enhanced absorption length kL, where k is the optical enhancement factor. Based on this definition, we have,

$$N(\lambda) = N_0\int_0^{kL} \alpha\exp(-\alpha x)dx = N_0\left[1-\exp(-\alpha kL)\right]. \quad (9)$$

Defining the quantum efficiency Q_{BR} of the cell on BR as $N(\lambda)/N_0$, then we have,

$$Q_{BR} = 1-\exp(-\alpha kL), \quad (10)$$

and,

$$k = -\frac{\ln(1 - Q_{BR})}{\alpha L}, \tag{11}$$

where αL is obtained from eq.(6) with the Q_{SS} data. As pointed out, the problem is over-simplified by the assumptions. In reality, there are always some optical losses at the metal/dielectric interface and top surface as well as in the doped layers. In addition, electrical losses by recombination in the intrinsic layers are also a factor for the accuracy of the estimation. Therefore, the estimation by this method gives the lowest limit of the optical enhancement as pointed above. In order to reduce the recombination losses, Q_{SS} and Q_{BR} data under a reverse bias should be used. The comparison to the calculation based on the Q_{ss} and Q_{BR} data under the short-circuit condition will provide the errors caused by the recombination process in the intrinsic layer.

2.3.3. Preliminary results

We have done some calculations of the optical enhancement factor *k* for a-SiGe:H single-junction solar cells. Figure 4 (a) shows a comparison of QE curves of a-SiGe:H single-junction solar cells made with the same recipe on a flat stainless steel substrate and a Ag/ZnO back reflector. The ratio of the two quantum efficiency curves is also plotted on the same figure. It is clear that the optical enhancement is mainly in the long wavelength region, because in the short wavelength region, the absorption coefficients are large enough for absorbing the light within one path through the thickness of the intrinsic layer. Fig. 4 (b) shows the calculated optical enhancement factor *k* using the procedure presented above, where two reflectivity *R* values at the semiconductor/stainless-steel were used. Normally, we use R=0.2 for the SS/a-Si:H interface. With this value, one can see that the maximum optical enhancement factor is about 25. The estimated optical enhancement factor strongly depends on the *R* value. If R=0.5 is used, the maximum optical enhancement factor can be as high as 30. In addition, the wavelength dependence of *R* is also a consideration for further improvement in the calculation accuracy.

2. 4. Summary

We have improved the a-SiGe:H bottom cells performance by optimizing the intrinsic a-SiGe:H layer deposition parameters such as hydrogen dilution and GeH_4 profiling. We also optimized the Ag/ZnO back reflectors to have high light trapping effect. We found that for Ag/ZnO back reflectors with a thinner ZnO layer, a textured Ag layer results in a higher short-circuit current density even if the plasmon absorption at the metal/dielectric interface is high for the textured Ag layer. The textured Ag provides high light scattering, which is the dominant factor for the back reflector. For thick ZnO, the flat and textured Ag layers showed a similar short circuit current density because with the increase of the ZnO thickness, the scattering by the textured ZnO is increased. At the same time, the absorption at the metal/dielectric interface is lower. In order to increase the short circuit current density further, we shall increase the texture at the ZnO/semiconductor interface. Further studies including chemical etching for texturing the ZnO surface is under way.

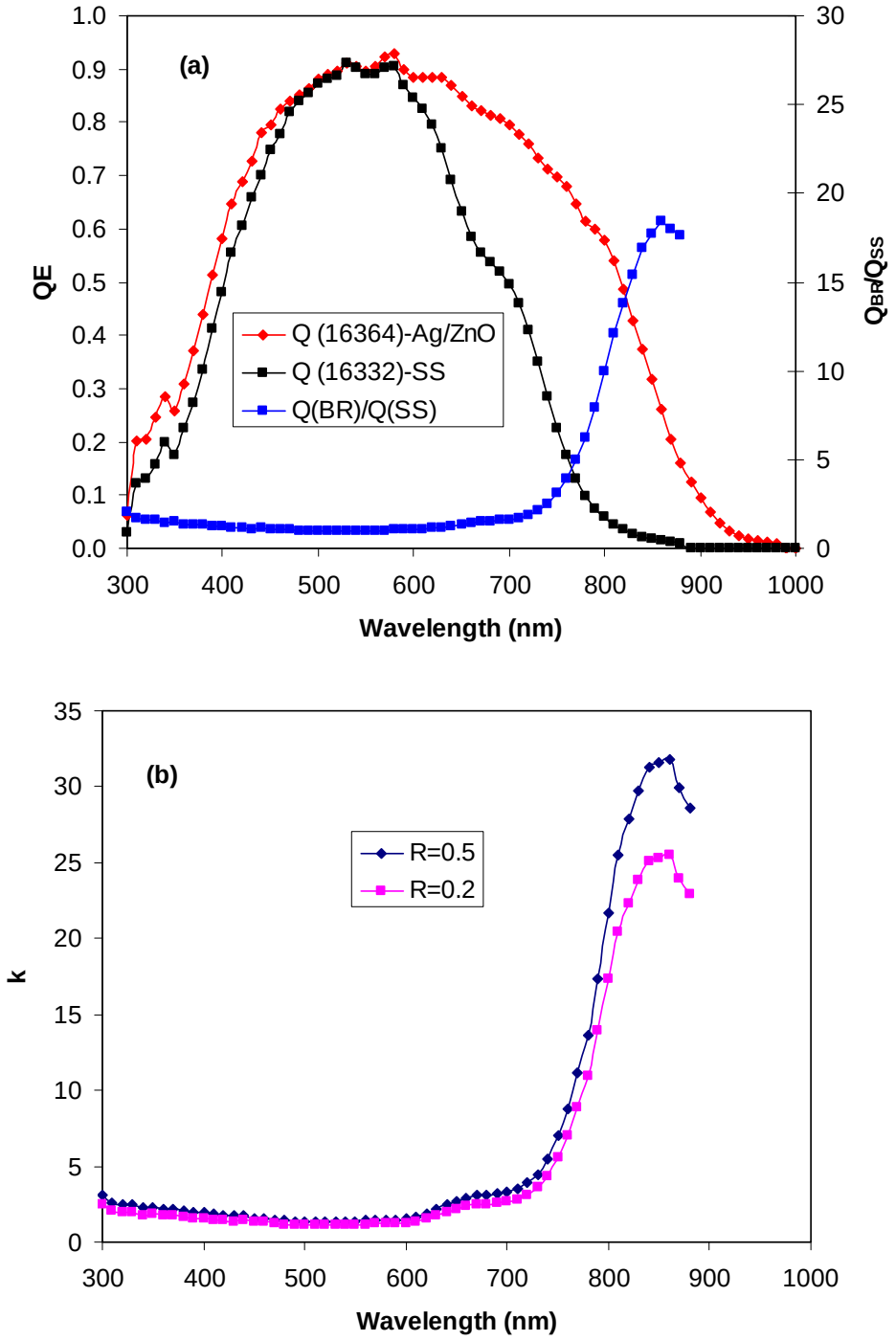

Figure 4. (a) Comparison of QE curves of a-SiGe:H single-junction cells deposited with the same recipe on a flat stainless steel substrate and a Ag/ZnO back reflector substrate; (b) the optical enhancement calculated using the procedure described in the text.

Reference

[1] A. Matsuda, Thin Solid Films, **337**, 1 (1999).

[2] J. Yang, A. Banerjee, K. Lord, and S. Guha, Proc. of 28th IEEE Photovoltaic Specialists Conference, Anchorage, AK, September 15-22, 2000 (IEEE, 2000), p. 742.

[3] T. Roschek, T. Repmann, J. Müller, B. Rech, H. Wagner, Proc. of 28th IEEE Photovoltaic Specialists Conference, Anchorage, AK, September 15-22, 2000, (IEEE, 2000), p. 150.

[4] D.V. Tsu, B.S. Chao, S.R. Ovshinsky, S. Guha, and J. Yang, Appl. Phys. Lett. **71**, 1317 (1997).

[5] J. Yang and S. Guha, Mater. Res. Soc. Symp. Proc. **557**, 239 (1999).

[6] E. Vallat-Sauvain, U. Kroll, J. Meier, and A. Shah, J. Appl. Phys. **87**, 3137 (2000).

[7] J.Y. Nasuno, M. Kondo, and A. Matsuda, Proc. of 28th IEEE Photovoltaic Specialists Conference (IEEE, Anchorage, Alaska, 2000), p.142.

[8] F. Finger, S. Klein, T. Dylla, A.L. Baia Neto, O. Vetterl, and R. Carius, Mater. Res. Soc. Symp. Proc. **715**, 123 (2002).

[9] B. Yan, G. Yue, J. Yang, S. Guha, D. L. Williamson, D. Han, and C.-S. Jiang, Appl. Phys. Lett. **85**, 1955 (2004).

[10] K. Lord, B. Yan, J. Yang, and S. Guha, Appl. Phys. Lett. **79**, 3800 (2001).

[11] J. Yang, K. Lord, B. Yan, A. Banerjee, S. Guha, D. Han, and K. Wang, Mater. Res. Soc. Symp. Proc. **715**, 601 (2002).

[12] J. Yang, A. Banerjee, and S. Guha, Solar Energy Materials & Solar Cells **78**, 597 (2003).

[13] H.J. Simon, D.E. Mitchell, and J.G. Watson, Am. J. Phys. **43**, 630 (1975).

[14] A. Banerjee and S. Guha, J. Appl. Phys. **69**, 1030 (1991).

[15] B. Yan, J. M. Owens, C.-S. Jiang, J. Yang, and S. Guha, Mater. Res. Soc. Symp. Proc. **862**, 603 (2005).

[16] E. Yablonovitch, J. Opt. Soc. Am. **72**, 899 (1982).